Research Article | Vol. 27, No. 13 | 24 Jun 2019 | OPTICS EXPRESS 19019
Optics EXPRESS

Transverse mode instability, thermal lensing and power scaling in Yb^{3+}-doped high-power fiber amplifiers

MICHALIS N. ZERVAS[1,2,*]

[1]Optoelectronics Research Centre, University of Southampton, Southampton SO17 1BJ, UK
[2]Advanced Laser Lab, ORC/SPI Lasers, Southampton, UK
*mnz@soton.ac.uk

Abstract: Transverse mode instability (TMI) is compared to thermal lensing (TL) power threshold and used to derive power scaling limits in high-power fiber amplifiers. The TMI power threshold is shown to be ~65% of the TL one and dominates power scaling. In addition to commonly used limiting effects, we introduce a bend-induced mechanical reliability criterion, which limits the maximum allowable cladding diameter to ~600μm. This also results in the introduction of a critical pump brightness, the minimum required pump brightness at which the maximum signal power is achieved. The maximum achievable power depends primarily on the choice of pumping wavelength, amplifier gain and heat coefficient. Maximum signal powers of ~28kW to ~38kW, for diode pumping (λ_p = 976nm), and ~35kW to ~52kW, for tandem pumping (λ_p = 1018nm), are predicted for single-mode fiber amplifiers operating at signal wavelength λ_s = 1070nm, when the amplifier gain is increased from 10dB to 20dB. For an amplifier gain of 10dB, the maximum achievable signal power varies from 85kW to 25kW for tandem pumping and 35kW to 20kW for diode pumping, when the heat coefficient varies from 1% to 15% and 5.5% to 20%, respectively. The corresponding critical pump brightness varies from ~0.50 W/(μm^2 sr) to ~0.14 W/(μm^2 sr) for tandem pumping and ~0.25 W/(μm^2 sr) to ~0.13 W/(μm^2 sr) for diode pumping.

1. Introduction

Cladding-pumped Yb^{3+}-doped high-power fiber lasers (HPFLs), in master-oscillator power amplifier (MOPA) configurations, have shown record single-moded diffraction-limited output powers in the range of 10kW [1,2]. Output power limits in cladding-pumped high-power fiber amplifiers (HPFAs) have been shown to be set by the pump brightness, optical nonlinearities (such as stimulated Raman (SRS) or Brillouin (SBS) scattering), optical damage, glass rapture or melting and thermal lensing (TL) [3,4].

The TL power threshold has been set arbitrarily to a level that results in pumped "hot" fiber mode-field diameter (MFD) $\omega_{TL} \approx 0.7 - 0.8\ \omega_0$, where ω_0 is the corresponding un-pumped ("cold") fiber MFD [3]. Therefore, its impact on power scalability is to some extend arbitrary and artificial. It has been shown that in diode-pumped HPFAs the output power limit is set to ~37kW, by a combination of pump brightness, SRS and TL limitations [3,4]. In the case of tandem pumping, the predicted power limit is increased to 70kW [5] and 68-97kW [6], limited by optical damage, SRS and TL effects.

More recently, transverse mode instability (TMI) [7] has been identified as a severely limiting power-dependent effect and its impact on power scaling has been considered [8–10]. In these studies, different TMI power threshold formulae were considered resulting in substantially different power scaling limits. In [8] the TMI threshold was considered to be reached at a fixed average heat load Q_0 = 34W/m, independent of core diameter [11], and predicted a diode-pumped power limit of 70kW, defined though by pump brightness, SRS

#364032 https://doi.org/10.1364/OE.27.019019
Journal © 2019 Received 3 Apr 2019; revised 13 May 2019; accepted 16 May 2019; published 21 Jun 2019

and TL. The power limit, however, was reduced to 10kW, when pump brightness, TMI and TL were considered. In [9] the TMI threshold scaled inversely with the core area and the diode-pumped power limit was set by pump brightness, SRS and TMI at ~28kW.

It should be noted that the aforementioned increased power limits were achieved with fiber-length/core-diameter combinations of ~20m/60μm [5], ~80m/130-220μm [6] and ~120m/260μm [8]. To date, however, the largest demonstrated active core is 135μm [12], and passive core diameter is 205μm [13], both achieved with microstructured large-pitch fibers and have to be kept straight over limited lengths of 1-2m. In addition, all previous power scaling investigations consider a fixed core pump absorption (Yb^{3+} concentration) and pump cladding absorption, which result also in large cladding diameters (>1mm). However, in practical HPFL systems to accommodate such ultra-long lengths the fibers should be bent in compact packages and the ramifications of bending such extra-large core and cladding diameter fibers have not been fully considered so far.

Following these results, it becomes apparent that efforts should be made to establish first a relation between the thermally driven TL and TMI thresholds, as well as, consider additional constraints imposed by the required long fiber lengths and large core diameters. Given that the majority of practical industrial or directed energy HPFL systems should preferably have minimum footprint, the additional constraints of mechanical reliability and mode field deformation of appropriately bent fibers should also be considered.

In this work, in Section 2 we first derive a simplified expression of the MFD shrinkage due to heat load and TL in HPFAs and compare it with published experimental results [14]. We also recast a recently derived simple TMI power threshold formula [15-17], in terms of laser efficiency (η_{laser}) and heat generation coefficient (η_{heat}), and compare it to the widely used TL power threshold [3]. In Section 3 we show representative power scaling results limited by the pump brightness, the onset of SRS/TMI and mechanical reliability, for diode-(DP) [18] and tandem-pumped (TP) [2,19,20] Yb^{3+}-doped HPFAs. In Section 4, we introduce the concept of critical pump brightness and derive the maximum achievable signal power as a function of pump brightness for different amplifier gains, laser efficiencies and dopant concentrations. In Section 5, we discuss the results and conclude. In Appendix A, we consider the bending-induced mechanical reliability and establish the maximum allowable cladding diameter. In Appendix B, we consider the bending-induced mode field deformation, and in Appendix C we summarize the different power limits due nonlinear, thermal and other effects. Finally, in Appendix D, we consider the heat-induced fundamental mode MFD shrinkage in optical fibers and compare it to the free-space case.

2. TL and TMI effects in optical fibers

In this section, we first consider the relation between thermal lensing, which is traditionally considered as one of the main power scaling limiting effects in HPFAs, and TMI.

2.1. TL-induced MFD shrinkage in optical fibers

We first derive a simplified formula for the MFD shrinkage due to thermal lensing and compare it with experimental results from the literature. The MFD diameter ω_0 in a step-index (SI) fiber is approximated by [21]:

$$\frac{\omega_0}{d_0} = 0.65 + \frac{1.619}{V^{3/2}} + \frac{2.879}{V^6} \tag{1}$$

where $d_0 = 2r_0$ is the core diameter, $V = \pi\left(d_0/\lambda_0\right)\sqrt{n_1^2 - n_2^2} \simeq \pi\left(d_0/\lambda_0\right)\sqrt{2n_2\Delta n}$, $\Delta n = n_1 - n_2$, with n_1 (n_2) being the core (cladding) refractive index, and λ_0 the signal wavelength (see Fig. 1(a)).

Steady-state thermal effects in HPFAs are described by the simplified steady-state heat equation $-\kappa\nabla_T^2\Delta T(z)=Q_0(z)$, where ∇_T^2 is the transverse Laplacian, ΔT is the temperature change, κ is the silica thermal conductivity. Q_0 is the heat power density (volumetric heat source), which in the case of an optically pumped amplifier is given by [22]:

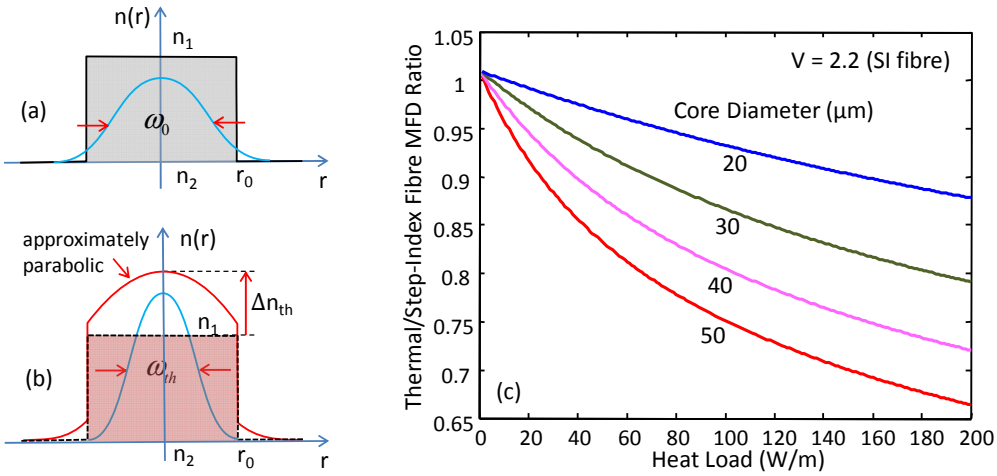

Fig. 1. Schematic of (a) "cold" step-index fiber, and (b) "hot" fiber quasi-parabolic refractive index profile; (c) "hot"/"cold" SI fiber MFD ratio.

$$Q_0 \simeq q_D dI_s/dz+\alpha_s I_s=(q_D g_s+\alpha_s)I_s \tag{2}$$

where $q_D=(\lambda_s/\lambda_p)-1$ is the quantum defect parameter, g_s is the saturated signal gain coefficient, α_s is the signal background loss, λ_s (λ_p) is the signal (pump) wavelength, and I_s the signal intensity. Thermal effects can also be quantified by the average heat load $\bar{Q}_{heat}$ approximated by [3]:

$$\bar{Q}_{heat}=\frac{P_{heat}}{L}=\frac{\eta_{heat}P_{pump}^{absorbed}}{L}=\left(\frac{\eta_{heat}}{\eta_{laser}}\right)\frac{P_{signal}^{extracted}}{L}=\left(\frac{\eta_{heat}}{\eta_{laser}}\right)\frac{P_s(L)}{L}\frac{G-1}{G} \tag{3}$$

where P_{heat} is the power dissipated into heat, L is the amplifier length, $P_{pump}^{absorbed}$ is the absorbed pump power, η_{heat} is the heat coefficient, η_{laser} is the laser efficiency and $P_{signal}^{extracted}$ is the extracted signal power ($P_{signal}^{extracted}=P_s(L)-P_s(0)$) and $G=P_s(L)/P_s(0)$ is the amplifier gain. For HPFAs for which $G\gg 1$, $\bar{Q}_{heat}\simeq(\eta_{heat}/\eta_{laser})(P_s/L)$.

Assuming a uniform heat load distribution across the fiber core, the thermally-induced core refractive index acquires a quasi-parabolic profile (see Fig. 1(b)) with maximum RI variation approximated by [23]:

$$\Delta n_{th} \approx \frac{\bar{Q}_{heat}\,(dn/dT)}{4\pi\kappa} \tag{4}$$

where (dn/dT) is the thermo-optic coefficient. In the case of thermally-induced quasi-parabolic RI profile, the fundamental mode MFD diameter ω_{th} is approximated by [21]:

Optics EXPRESS

$$\frac{\omega_{th}}{d_0}=\frac{\sqrt{2}}{V_{th}^{1/2}}+\frac{0.23}{V_{th}^{3/2}}+\frac{18.01}{V_{th}^{6}} \tag{5}$$

where $V_{th}=\pi\left(d_0/\lambda_0\right)\sqrt{2n_2\Delta n(1+\Delta n_{th}/\Delta n)}=V\sqrt{1+\Delta n_{th}/\Delta n}$. The "hot" to "cold" MFD ratio (ω_{th}/ω_0) versus the heat load is plotted in Fig. 1(c), for different core diameters and V = 2.2. It is shown that for all core diameters the MFD "shrinks" as the heat load increases. The "hot" fiber MFD shrinkage is more pronounced in larger core diameter fibers. This implies that large mode area (LMA) fibers are expected to be more prone to thermal effects.

2.2. TL and TMI power limits

In the literature [3], TL limit is considered as the power above which a Gaussian beam propagating in free space negates diffraction and starts self-guiding under the influence of a thermally-induced quasi-parabolic RI profile. Using an ABCD matrix analysis, the derived TL power limit is then given by Eq. (24), namely:

$$P_{out}^{TL}=\frac{2\pi\kappa}{\left[\eta_{heat}/(\eta_{laser}L)\right](dn/dT)}\left(\frac{\lambda_0}{d_0}\right)^2 \tag{6}$$

and corresponds to a reduction of the beam initial MFD by a factor of 0.7-0.8. κ is the silica thermal conductivity and dn/dT the thermo-optic coefficient.

A TMI power threshold has been derived by carrying out a stability analysis of the fundamental (LP_{01}) mode amplification process, in the presence of heat load induced by the amplifier quantum defect. The TMI limit or threshold, in this case, corresponds to the power above which a small spatial perturbation (e.g. in the form of LP_{11} mode) increases exponentially [15–17]. The derived TMI power limit, in this case, is given by Eq. (23). In HPFAs, heat generation is dominated by the quantum-defect contribution and, therefore, we can set $\alpha_s'\simeq q_D g_s$ ($\alpha_s \ll q_D g_s$). Expressing $\bar{Q}_{heat}=Q_0\pi r_0^2$ and using Eqs. (2) and (3), we approximate. This approximation is more appropriate for the case of backward pumping. From Eq. (24) then the TMI power limit takes the simplified form:

$$P_{out}^{TMI}=\frac{\kappa U_\varepsilon^2\left(U_\varepsilon^2-U_s^2\right)}{2\pi n_{eff}\left[\eta_{heat}/(\eta_{laser}L)\right](dn/dT)}\left(\frac{\lambda_0}{d_0}\right)^2, \tag{7}$$

which now can be compared directly with the TL power limit in Eq. (6). n_{eff} is the fundamental mode effective index and $U_s(U_\varepsilon)$ is the normalized transverse wavenumber for the fundamental (higher-order) fiber mode. Despite their fundamentally different physical character and derivation method, both the TL and TMI limits show the same dependence [$\propto (\lambda_0/d_0)^2$] on signal wavelength ($\lambda_0$), core diameter ($d_0$), laser efficiency ($\eta_{\text{laser}}$), heat generation coefficient (η_{heat}) and fiber length L. In addition to core diameter and the parameters shown in Eq. (7), it has been shown experimentally (see Fig. 1 in [16]) that the TMI threshold depends strongly also on the signal linewidth. The simplified TMI threshold formula in Eq. (7) applies to broad linewidth operation.

However, it should be emphasized that TMI results in detrimental beam break-up, while TL results simply in 20-30% MFD shrinkage. The latter is not damaging, although it can decrease the threshold of other nonlinear effects, such as SRS. In some cases, though, like in large-pitch fibers, TL can be beneficial to some extend as it can initially stabilize the beam shape and contribute to more robust guiding [24,25].

From Eqs. (6) and (7), it is deduced that the TMI/TL power limit ratio is given by

Optics EXPRESS

$$\frac{P_{out}^{TMI}}{P_{out}^{TL}} = \frac{U_\varepsilon^2 (U_\varepsilon^2 - U_s^2)}{4\pi^2 n_{eff}} \tag{8}$$

and depends only on the fiber core V-number. For $V = 3$, $P_{out}^{TMI} / P_{out}^{TL} \approx 0.6$. Figure 2 compares TMI and TL power limits as a function of fiber core diameter, for $V = 3$, $\eta_{heat} = 0.3$ and $\eta_{laser} = 0.7$. The other parameters are given in Appendix C. As expected, P_{out}^{TMI} is ~40% lower than P_{out}^{TL}. This is an important finding and it is expected to redefine the limits in HPFA power scaling (see Section 3).

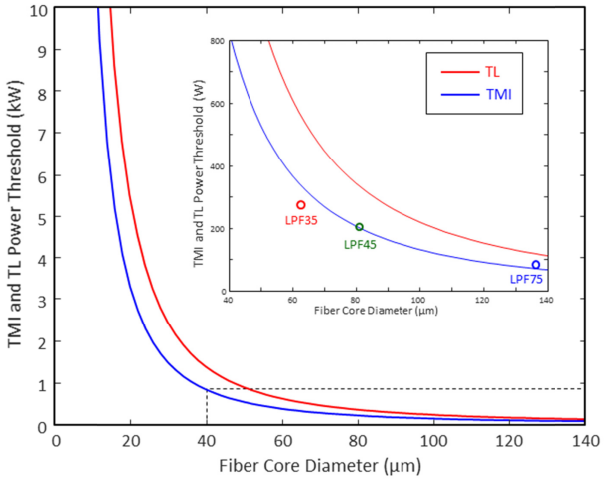

Fig. 2. TMI and TL power limits in fibers with $V = 3$, $\eta_{heat} = 0.3$ and $\eta_{laser} = 0.7$. The other parameters are given in Appendix C. The inset zooms into the dashed area and superimposes experimental data (open circles) [14].

2.3. MFD shrinkage & TL / TMI power limits comparison - experimental validation

As already mentioned, in previous studies the TL power limit (see Eq. (6)) corresponds to ~20-30% MFD reduction of a Gaussian beam propagating in free space [3]. Using the simplified analysis and results of Sections 2.1 and 2.2 in Appendix D we have shown that at the TL power limit (i.e. $P_s = P_{out}^{TL}$) and typical "cold" fiber V = 3-4, the "hot"-to-"cold" MFD ratio of the fundamental fiber mode is approximated by $\omega_{th}^{TL} / \omega_0 \simeq \sqrt{2/(V\sqrt{2})} \simeq 0.7 - 0.8$, which is similar to the free-space case.

To verify the theoretical predictions regarding TMI and TL power limits, given by Eqs, (6)–(8), and the dependence of "hot" fiber fundamental mode MFD shrinkage on extracted power, or equivalently, on average heat load given by Eqs. (3)–(5), we have compared our findings with published experimental results. In Ref [14], MFD variations with extracted signal power and TMI power thresholds have been measured in a range of large-pitch microstructured fibers (LPFs) with different core diameters. The LPFs are drawn from the same preform and, therefore, have the same Yb^{3+} ion concentration, core/cladding ratio and length of L = 1.2m.

Figure 3 replots the results for three LPFs with fiber core diameters of 136μm (LPF75-blue open circles), 80μm (LPF45-green open circles) and 63μm (LPF35-red open circles)) [14]. It is shown that the output MFD diameter decreases with extracted power, due to increasing level of thermal lensing. For each fiber, the measurements are limited by the onset of TMI, beyond which the output beam is distorted dynamically by the presence of higher-

Optics EXPRESS

order modes (HOMs) and the MFD cannot be defined. The corresponding fundamental mode MFD diameter (ω_{th}) variation with extracted power (Eqs.. (3)–(5)) for each fiber (solid lines) is also plotted, showing a very good agreement. The used parameters were $V = 3$, $\eta_{heat} = 0.3$ and $\eta_{laser} = 0.7$. The other parameters are given in Table 1 in Appendix C. The dashed lines denote the 30% reduction from the "cold" MFD value (i.e. $\omega_{th}^{TL}/\omega_0 \simeq 0.7$), which corresponds to the TL limit. The red arrows denote the corresponding TL powers (P_{out}^{TL}), while the blue arrows denote the expected TMI limits (P_{out}^{TMI}) with $P_{out}^{TMI} \approx 0.65 P_{out}^{TL}$. It is observed that for LPF75 and LPF45 the predicted TMI powers agree very well with the experimentally obtained ones. Also, the used ratio $P_{out}^{TMI}/P_{out}^{TL} \approx 0.65$ is in very good agreement with the theoretically predicted value of 0.6. In the case of LP35, the experimental TMI limit is slightly lower than the predicted value.

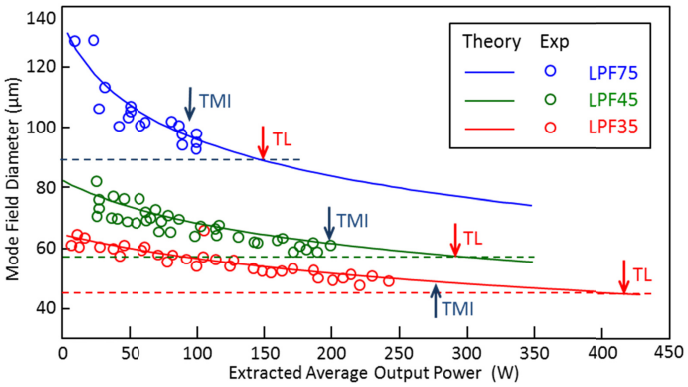

Fig. 3. MFD shrinkage with extracted power. Open circles: experimental data [14]; blue: LPF75, green: LPF45, red:LPF35. Solid lines: Theory (Eq. (5)) with $V = 3$, $\eta_{heat} = 0.3$ and $\eta_{laser} = 0.7$ and $d_0 = 136\mu m$ (blue); $80\mu m$ (green); $63\mu m$ (blue). Dashed lines correspond to 70% "hot"-to"-cold" MFD shrinkage ($\omega_{th}/\omega_0 = 0.7$). Red and blue arrows denote the TL and TMI powers, respectively, for which $P_{TMI}/P_{TL} = 0.65$.

In all cases, it is observed that TMI sets in well before the conventional TL limit is reached, following closely a $(1/d_0)^2$ dependence. The inset of Fig. 2 zooms into the dashed area and superimposes experimental data (stars) [14], showing again a very good agreement for LPF75 and LPF45. For LPF35 ($d_0 = 63\mu m$), however, the experimental TMI power limit is again lower than the theoretical prediction. In addition to thermal load, TMI threshold is known to be lowered by a number of other factors such as additional backreflections [26], amount of the input higher-order mode [27] and photodarkening [28]. These effects are not included in our simplified analysis and could contribute to the observed discrepancy. At this point, it should be mentioned that using Eq. (3), the alternative TMI power threshold, which is considered to occur at a fixed average heat load of $\bar{Q}_{heat} = 34 W/m$ [11] and was used in [8] to evaluate the impact of TMI on power scaling, takes the simplified form $P_{TMI2} = 34(\eta_{laser}/\eta_{heat})L$. In this case, the predicted TMI power threshold would have been ~105W, independent of the core diameter and not matching the observed experimental trend.

Finally, independently in [29] M.M. Johansen et.al. using a semi-analytical model have calculated numerically both the MFD shrinkage and TMI power threshold as a function of heat load. Using again $\omega_{th}^{TL}/\omega_0 \simeq 0.7-0.8$ as the thermal lensing threshold criterion, from Figs. 4 and 6 in [29] it is deduced that the TMI/TL average-heat-load ratio is $\bar{Q}_{heat}^{TMI}/\bar{Q}_{heat}^{TL} \simeq 75/120 = 0.63$. Given the linearity between signal power and average heat load, this corresponds to $P_{out}^{TMI}/P_{out}^{TL} \approx 0.63$ in excellent agreement with our results in this section.

Optics EXPRESS

Experimental data in Fig. 3 were used primarily to show the relation between TL and TMI thresholds and compare them with the simplified formulae (6) and (7). The TMI threshold is inversely proportional to the saturated amplifier gain g_s through $\alpha_s' \simeq q_D g_s \simeq \eta_{heat}/(\eta_{laser} L)$ and, therefore, it is a multi-dimensional function of the pump/signal wavelength, input signal power, dopant concentration, and cladding diameter. In Fig. 5 of Ref [16], it is shown that the simplified TMI threshold formula agrees with experimental data up to multi-kW level for a large range of core diameters and amplifier gains.

3. Power scaling limits

We now investigate the power scaling limits in HPFAs, taking into account the newly developed TMI threshold formula and the constraints into maximum allowable cladding diameter due to fiber mechanical reliability, in addition to the nonlinear and other limits summarized in Appendix C. Throughout the analysis the fiber V-number is fixed to $V = 3$.

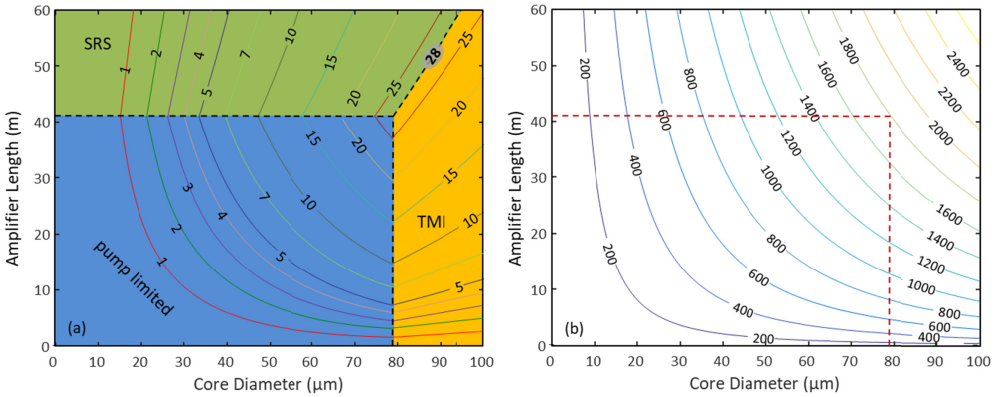

Fig. 4. Contour plots of (a) power lower limits (in kW) due to pump brightness (blue area), SRS (green area) and TMI (orange area); and (b) required cladding diameter (in μm) as a function of amplifier length and core diameter. The parameters are similar to Ref [3]. (see Table 1 in Appendix C and B_p = 0.02W/μm^2/sr; η_{laser} = 0.85; η_{heat} = 0.10, G = 10dB).

Figure 4(a) shows contour plots of the power scaling limits (in kW) due to the nonlinear and other effects with parameters similar to [3], i.e. B_p = 0.02W/μm^2/sr; η_{laser} = 0.85; η_{heat} = 0.10, all related to 976nm diode pumping and lasing at ~1070nm. It is shown that the power scaling in this case is limited by pump power (blue area), SRS (green area), and TMI (orange area) in place of the previously dominating thermal lensing. It is noted that due to the lower TMI threshold, the maximum achievable power is reduced from ~37kW in [3] to ~28kW.

From Fig. 4(a), three border (dashed) lines are identifiable. The border line between pump- and SRS-limited powers is obtained by setting $P_{out}^{pump} = P_{out}^{SRS}$ (see Eqs. (22) and (26)), and it is given by:

$$L_{pump-SRS} = \frac{4\Gamma}{NA}\sqrt{\frac{\ln(G)A_p}{\pi g_R \eta_{laser} B_p \alpha_{core}}} \tag{9}$$

which is independent of the core diameter. The border line between pump- and TMI-limited powers is obtained by setting $P_{out}^{pump} = P_{out}^{TMI}$ (see Eqs. (22) and (6)), and it is given by:

$$d_{pump-TMI} = \sqrt[4]{\frac{2\kappa U_\varepsilon^2 \left(U_\varepsilon^2 - U_s^2\right)\lambda_0^2 A_p}{\pi^3 n_{eff}\eta_{heat}\left(dn/dT\right)B_p \alpha_{core} NA^2}} \tag{10}$$

Optics EXPRESS

which is independent of the amplifier length. For $L > L_{\text{pump-SRS}}$ and $d_0 > d_{\text{pump-TMI}}$, the border line between TMI- and SRS-limited powers corresponds to $P_{out}^{TMI} = P_{out}^{SRS}$ (see Eqs. (6) and (26)), and it is given by:

$$L_{TMI-SRS} = \frac{2\pi d_0^2}{\lambda_0}\sqrt{\frac{2n_{eff}\eta_{heat}\left(dn/dT\right)\Gamma^2\ln\left(G\right)}{\eta_{laser}\kappa U_\varepsilon^2\left(U_\varepsilon^2 - U_s^2\right)g_R}} \tag{11}$$

Along this border the maximum achievable power is obtained, given by:

$$P_{TMI-SRS}^{\max} = \lambda_0\sqrt{\frac{2\eta_{laser}\kappa U_\varepsilon^2\left(U_\varepsilon^2 - U_s^2\right)\Gamma^2\ln(G)}{n_{eff}\eta_{heat}\left(dn/dT\right)g_R}} \tag{12}$$

The required minimum amplifier length and core diameter to obtain the maximum achievable output power are given by Eqs. (9) and (10), respectively. In the case of Fig. 4(a), the corresponding values are 41m and 78μm, respectively. Figure 4(b), on the other hand, plots the required cladding diameter (in μm), as given by Eq. (23), required for the power levels plotted in Fig. 4(a) to be achieved. It is shown that the maximum achievable power of ~28kW requires a minimum cladding diameter of 1.6mm. With such cladding dimensions these structures can hardly qualify as "standard" bendable optical fibers and the implications on power scaling will be considered next.

3.1 Fiber mechanical reliability considerations

In all the previous power scaling investigations, fixed core (α_{core}) and total (A_{p}) pump absorption were considered and as a result large core diameters were accompanied by large cladding diameters (>1mm) and long fiber lengths (>>10m) [3–6,8]. Given that most practical industrial or directed energy HPFL systems should preferably have minimum footprint, the additional constraints of mechanical reliability of bent large-cladding-diameter fibers should be considered [30]. Figure 9 in Appendix A shows the calculated failures-in-time (FIT) as a function of fiber bending diameter (D_{bend}), for different cladding diameters. The fiber is assumed to have undergone minimum proof testing and the failure time is 20years [31,32]. Assuming a maximum bending diameter D_{bend} = 1m, the maximum allowable cladding diameter is d_{mech} = 600μm. This additional limit will be used in the subsequent calculations. From Eq. (23), the *mechanical reliability border line* can be defined as:

$$L_{mech} = \frac{A_p d_{mech}^2}{\alpha_{core} d_0^2} \tag{13}$$

When within the pump-limited (blue) region, the maximum achievable signal power, along the mechanical reliability border line, is given by:

$$P_{pump}^{\max} = \frac{1}{4}\eta_{laser} B_p \pi^2 NA^2 d_{mech}^2 \tag{14}$$

Optics EXPRESS

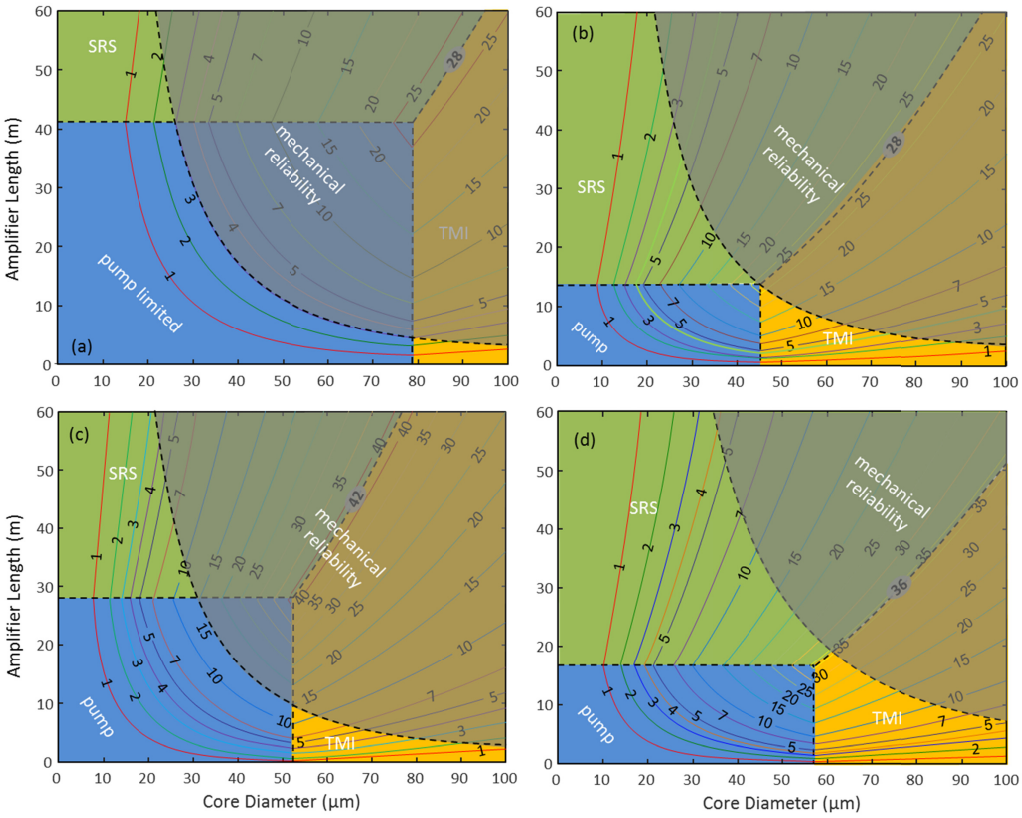

Fig. 5. Contour plots of power limits (in kW) due to pump brightness (blue area), SRS (green area) and TMI (orange area). The mechanical-reliability dominated parameter space (grey area) is also shown. (a) DP with B_p = 0.02W/μm^2/sr; η_{laser} = 0.85; η_{heat} = 0.10, G = 10dB; (b) DP with B_p = 0.18W/μm^2/sr; η_{laser} = 0.85; η_{heat} = 0.10, G = 10dB; (c) DP with B_p = 0.2W/μm^2/sr; η_{laser} = 0.85; η_{heat} = 0.10, G = 23dB; (d) TP with B_p = 0.3W/μm^2/sr; η_{laser} = 0.85; η_{heat} = 0.06, G = 10dB. Core pump absorption: (a)-(c) α_{core} = 250dB/m, (d) 100dB/m.

Figure 5(a) replots the power limits (in kW) shown in Fig. 4(a). However, when we consider the additional mechanical reliability constraint, the maximum power reduces from 28kW to 3kW! As shown in Fig. 5(b), increasing the pump brightness to B_p = 0.18W/(μm^2 sr) reduces considerably the fiber length and core diameter requirements and results in a maximum power of ~28kW even when the mechanical reliability constraint is considered. It should be pointed out that at this pump brightness the dominant power limits (i.e. pump/SRS, pump/TMI, SRS/TMI and mechanical reliability) all acquire the same maximum achievable power level. This leads to the critical pump brightness introduced in Section 4.

In Fig. 5(c) it is shown that increasing the amplifier gain to 23dB increases the SRS/TMI-limited power to ~42kW. However, when we impose the mechanical reliability limit the maximum power reduces to ~15kW. It should be mentioned that in this case, a 20μm core fiber, ~30m long amplifier provides a maximum of ~5kW SRS limited, in close agreement with recent experimental results with similar parameters [33].

Finally, in the case of tandem pumping, with parameters B_p = 0.3W/(μm^2 sr); η_{laser} = 0.85; η_{heat} = 0.06 λ_p = 1018nm, the maximum achievable power is increased to ~36kW limited by SRS/TMI. In this case, imposition of the mechanical reliability limit has no effect on the maximum achievable power, which is achieved with a minimum fiber length of ~17m and a minimum core diameter of ~57μm. However, as discussed in Appendix B, for a more practical core diameter of ~35-40μm the maximum achievable power reduces to ~15-20kW.

Optics EXPRESS

It should be mentioned also that a 30μm core fiber, 10dB gain, ~15m long amplifier is expected to provide a maximum of ~10kW pump/SRS limited signal power, in close agreement with the record experimental result in [2].

4. Pump brightness requirements

Pump brightness, along with the mechanical reliability imposed maximum cladding diameter, are among the most important parameters in defining the power scaling limits in HPFAs. While the TMI/SRS-limited power, given by Eq. (12), is independent of pump brightness (B_p), the pump-limited power, given by Eq. (14), is proportional to B_p. We can define a *critical pump brightness* B_p^{crit}, which is the minimum brightness for which $P_{pump}^{\max} = P_{TMI-SRS}^{\max}$. This corresponds to the case shown in Fig. 5(b), where the pump/SRS, pump/TMI, SRS/TMI and mechanical reliability power limits coincide. From Eqs. (12) and (14), the critical pump brightness is then given by:

$$B_p^{crit} = \frac{4\lambda_0 U_\varepsilon \Gamma}{\pi^2 NA^2 d_{mech}^2}\sqrt{\frac{2\kappa\left(U_\varepsilon^2 - U_s^2\right)\ln(G)}{n_{eff}\eta_{laser}\eta_{heat}\left(dn/dT\right)g_R}} \tag{15}$$

The critical pump brightness depends on the maximum allowable cladding diameter d_{mech}. It also depends on the amplifier gain, laser efficiency and heat coefficient, in addition to other fiber parameters and thermo-optic constants.

The critical pump brightness defines the dependence of maximum achievable signal power and the required minimum core diameter, fiber length and cladding diameter on pump brightness.

A. Maximum Signal Power ($P_s^{\max}$): It is easily deduced that the maximum achievable signal power is given by:

$$P_s^{\max} = \begin{cases} P_{pump}^{\max} & ;\ B_p < B_p^{crit} \\ P_{TMI-SRS}^{\max} & ;\ B_p \geq B_p^{crit} \end{cases} \tag{16}$$

where $P_{pump}^{\max}$ and $P_{TMI-SRS}^{\max}$ are given by Eqs.. (14) and (12), respectively.

B. Minimum Core Diameter ($d_0^{\min}$): When $B_p < B_p^{crit}$, the mechanical reliability border line overlaps with the pump-limited region (see Figs. 5(a) and (c)) and there is a range of fiber core-diameter/length combinations available. The minimum core diameter $d_{mech-SRS}$, however, is obtained by setting $L_{mech} = L_{pump-SRS}$, which when using Eqs. (9) and (13) takes the form:

$$d_{mech-SRS} = d_{mech}\sqrt[4]{\frac{\pi\eta_{laser}g_R NA^2 A_p B_p}{16\Gamma^2 \ln(G)\alpha_{core}}} \tag{17}$$

When $B_p \geq B_p^{crit}$, on the other hand, the mechanical reliability border line does not overlap with the pump-limited region and instead it intersects the TMI/SRS border line $L_{TMI-SRS}$ (see Eq. (11) and Fig. 5(d)). However, since the maximum signal power is constant along this border, the minimum core diameter is given by the corresponding $d_{pump-TMI}$, given by Eq. (10). Overall, the minimum core diameter is given by:

$$d_0^{\min} = \begin{cases} d_{mech-SRS} & ;\ B_p < B_p^{crit} \\ d_{pump-TMI} & ;\ B_p \geq B_p^{crit} \end{cases} \tag{18}$$

Optics EXPRESS

C. Minimum Fiber Length ($L_{\min}$): Following the same reasoning, for any pump brightness the corresponding minimum fiber length is obtained by setting $L_{\min} = L_{pump-SRS}$ and it is given by Eq. (9).

D. Minimum Cladding Diameter ($d_{clad}^{\min}$): The minimum cladding diameter is given by Eq. (23) by substituting $d_0^{\min}$ from Eq. (18) and $L_{\min} = L_{pump-SRS}$ from Eq. (9). It is then straightforward to show that $d_{clad}^{\min}$ is given by:

$$d_{clad}^{\min} = \begin{cases} d_{mech} & ;\ B_p < B_p^{crit} \\ d'_{clad} & ;\ B_p \geq B_p^{crit} \end{cases} \tag{19}$$

where

$$d'_{clad} = \sqrt[4]{\frac{32\kappa\Gamma^2 U_\varepsilon^2 \left(U_\varepsilon^2 - U_s^2\right)\lambda_0^2 \ln(G)}{n_{eff} g_R \eta_{laser} \eta_{heat} \left(dn/dT\right)\pi^4 NA^4 B_p^2}} \tag{20}$$

Figure 6(a) plots the maximum achievable signal power (right axis) and minimum fiber length (right axis) as a function of pump brightness for diode pumping (DP – red lines) and tandem pumping (TP-blue lines). For DP the parameters were η_{heat} = 0.10, η_{laser} = 0.85, α_{core} = 250dB/m, while for TP they were η_{heat} = 0.06, η_{laser} = 0.90, and α_{core} = 100dB/m. In both cases, the amplifier gain was G = 10dB. The rest of the parameters are shown in Table 1. For $B_p < B_p^{crit}$, the maximum signal power is pump limited and increases linearly with the pump brightness. For $B_p \geq B_p^{crit}$, on the other hand, it is TMI/SRS limited and it is independent of the pump brightness. Tandem pumping shows larger critical pump brightness due to smaller η_{heat}, (see Eq. (15), and larger slope due to larger η_{laser} (see Eq. (14). As a consequence, TP results in larger maximum signal power (~37kW) compared to DP (~28kW). The minimum required fiber length, on the other hand, decreases monotonically with B_p ($\propto B_p^{-0.5}$), for both TP and DP. TP results in longer fiber lengths because of the smaller absorption cross-section at 1018nm as compared to 976nm pumping.

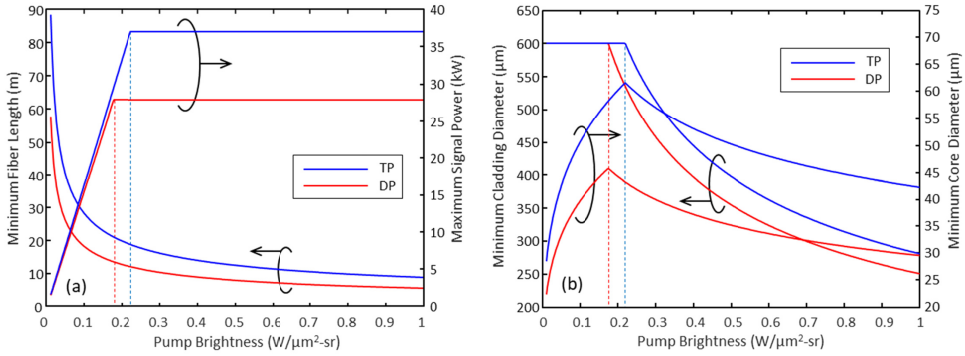

Fig. 6. (a), Maximum signal power (right axis), minimum fiber length (left axis), and (b) Minimum core diameter (left axis), minimum cladding diameter (right axis). Diode pumping (DP): η_{heat} = 0.10, η_{laser} = 0.85, α_{core} = 250dB/m; Tandem pumping (TP): η_{heat} = 0.06, η_{laser} = 0.90, α_{core} = 100dB/m. Amplifier gain G = 10dB (vertical dashed lines show the corresponding critical pump brightness).

Figure 6(b) plots the required minimum cladding diameter (left axis) and minimum core diameter (right axis) for TP (red lines) and DP (blue lines), as a function of pump brightness. The required minimum core/cladding diameters are shown to vary non-monotonically with B_p. For $B_p < B_p^{crit}$, the minimum core diameter increases with B_p ($\propto B_p^{0.25}$). For $B_p \geq B_p^{crit}$, on the

Optics EXPRESS

other hand, the minimum core diameter decreases with B_p ($\propto B_p^{-0.25}$). The minimum required core diameter peaks at a higher value for TP (~62μm), as compared to DP (~46μm). In Fig. 6(b), it also shown that for $B_p < B_p^{crit}$ the minimum cladding diameter remains constant at d_{mech}, for both DP and TP. For $B_p \geq B_p^{crit}$, on the other hand, the minimum cladding diameter decreases with B_p ($\propto B_p^{-0.5}$), for both DP and TP. From a physical point of view, since for $B_p < B_p^{crit}$ the cladding diameter remains fixed and the fiber length decreases with B_p, the core diameter increases in order to maintain a total cladding pump absorption of A_p = 20dB. For the same reason when $B_p \geq B_p^{crit}$ both fiber length and cladding diameter decrease and result in an appropriate core diameter decrease. This can also be verified analytically by considering $A_p = \alpha_{core} (r_0 / r_{clad})^2 L$ and substituting Eqs. (9), (18) and (19).

From Figs. 6(a) and (b) it is deduced that although increasing the pump brightness above the critical value does not result in further signal power increase, nevertheless it reduces considerably the requirements in fiber core/cladding diameters and length leading to more robust and manufacturable HPFLs.

Figure 7(a) plots the maximum signal power (right axis) and minimum fiber length (left axis), while Fig. 7(b) plots the required minimum cladding diameter (left axis) and minimum core diameter, respectively, for diode pumping (η_{heat} = 0.10, η_{laser} = 0.80, α_{core} = 250dB/m). Figures 7(c) and (d) plots the corresponding parameters for tandem pumping (η_{heat} = 0.06, η_{laser} = 0.85, α_{core} = 100dB/m). In both cases, the amplifier gain (G) is set to 10dB (blue lines), 15dB (green lines) and 20dB (red lines). In the DP case, increasing the amplifier gain from 10dB to 20dB increases the maximum signal power from ~27kW to ~38kW. The critical pump brightness increases from 0.18 W/(μm^2 sr) to 0.26 W/(μm^2 sr), while the required core diameter reduces from ~46μm to ~42μm. In the TP case, the same amplifier gain variation increases the maximum signal power from ~37kW to ~52kW. The critical pump brightness increases from 0.22 W/(μm^2 sr) to 0.32 W/(μm^2 sr), while the required core diameter reduces from ~62μm to ~55μm. These results show that increasing the amplifier gain increases the maximum achievable signal power, as a direct result of the resulting increase in critical pump brightness ($B_p^{crit} \propto [\ln(G)]^{+0.5}, (\eta_{heat})^{-0.5}$ - see Eq. (15)).

From Eq. (12), it is obvious that the maximum achievable signal power depends explicitly on the heat coefficient η_{heat}. The heat coefficient depends on the choice of the pump and signal wavelengths [34], as well as, additional effects such as the signal background loss due to glass impurities or photodarkening [28,35]. The heat coefficient, therefore, can vary from a minimum value determined by the quantum defect ($\eta_{heat}^{min} = q_D^{min}$) to a maximum value $\eta_{heat}^{max} = 1 - \eta_{laser}$ (assuming negligible signal scattering, HOM excitation and other pump losses).

Optics EXPRESS

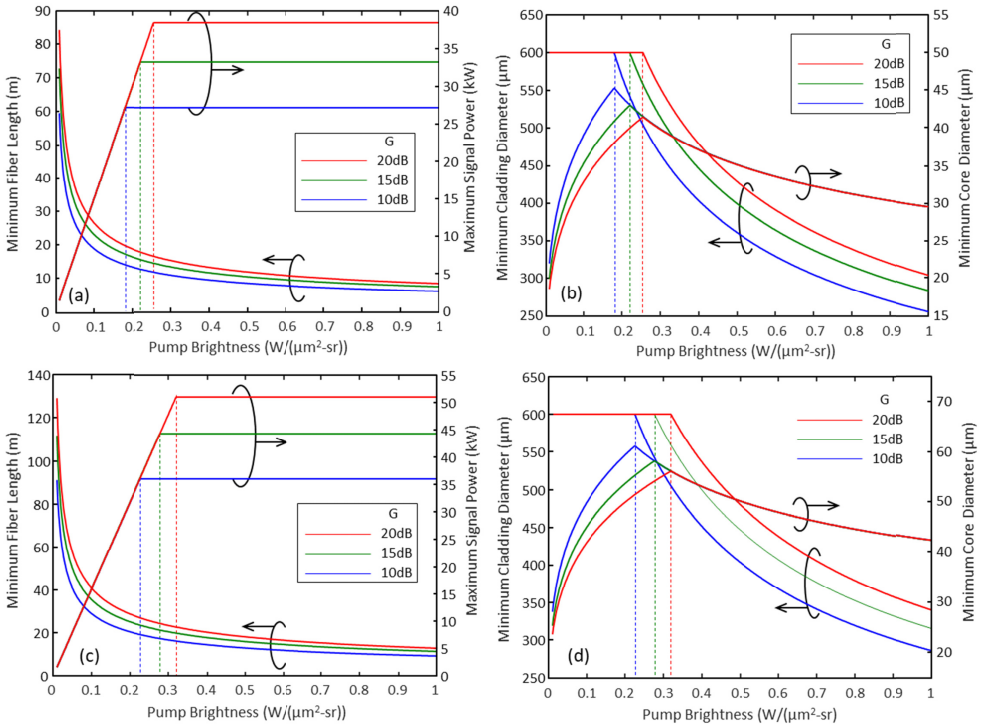

Fig. 7. (a) maximum signal power, (b) minimum fiber length/core diameter for diode pumping (η_{heat} = 0.10, η_{laser} = 0.80, α_{core} = 250dB/m); (c) maximum signal power, (d) minimum fiber length/core diameter for tandem pumping (η_{heat} = 0.06, η_{laser} = 0.85, α_{core} = 100dB/m). Amplifier gain G = 10dB (blue lines), 15dB (green lines) and 20dB (red lines).

Figure 8 plots (a) the maximum achievable signal power, (b) critical pump brightness, (c) corresponding core diameter and (d) fiber length as a function of heat coefficient, for diode pumping (red lines) and tandem pumping (blue lines). In the DP case (λ_p = 976nm), $\eta_{heat}^{min} = q_D^{min}$ varies from ~5.5% to ~12% when the signal varies from λ_s = 1030nm to 1090nm (indicated by red vertical arrows). Assuming $\eta_{laser.}$ = 0.80 results in η_{heat}^{max} = 0.20. In the TP case (λ_p = 1018nm), η_{heat}^{min} varies from ~1.2% to ~7% when the signal varies from λ_s = 1030nm to 1090nm (indicated by blue vertical arrows). In this case we assume $\eta_{laser.}$ = 0.85 and, therefore, η_{heat}^{max} = 0.15. In both cases, the amplifier gain is G = 10dB and the cladding diameter is 600μm. Under these conditions, the maximum achievable signal power varies from 85kW to 25kW for TP, and 35kW to 20kW for DP. The corresponding critical pump brightness varies from ~0.50 W/(μm^2 sr) to ~0.14 W/(μm^2 sr) for TP, and ~0.26 W/(μm^2 sr) to ~0.13 W/(μm^2 sr) for DP.

Optics EXPRESS

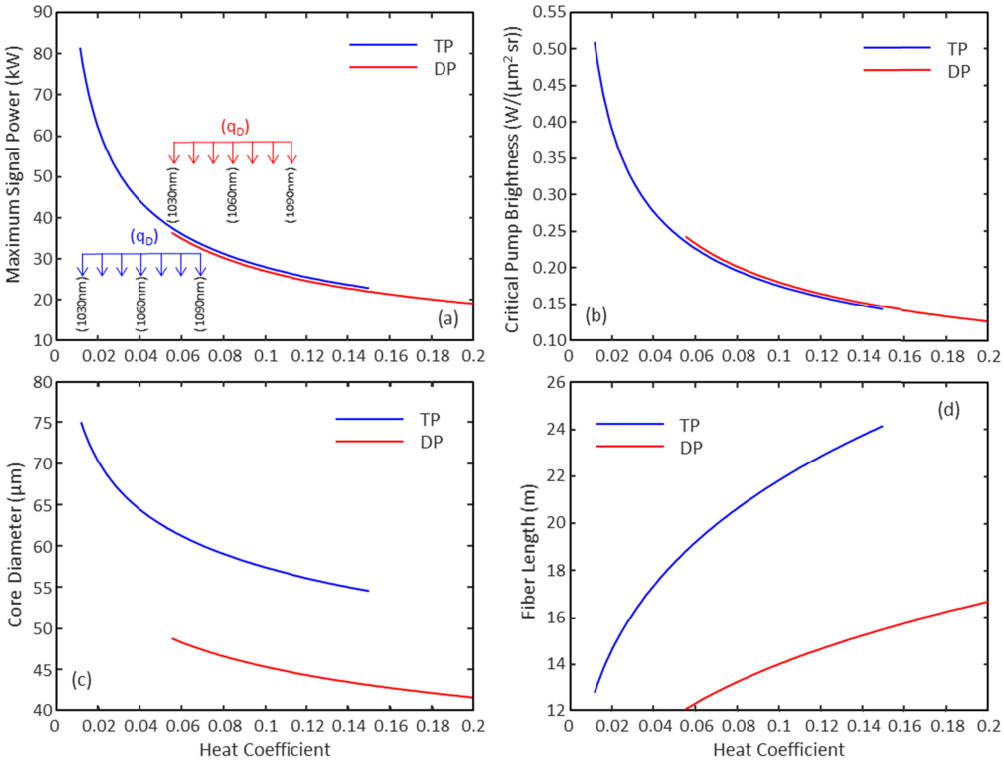

Fig. 8. (a) the maximum achievable signal power, (b) the critical pump brightness, (c) corresponding core diameter and (d) the fiber length as a function of heat coefficient, for diode pumping (η_{laser} = 0.80 - red lines) and tandem pumping (η_{laser} = 0.85 - blue lines). G = 10dB.

Variations in laser efficiency (η_{laser}) result in smaller variations in maximum laser power and the required core diameters. For DP and G = 10dB, varying the laser efficiency from 75% to 85% increases the maximum signal power from ~26kW to ~28kW. Similarly, for TP varying the laser efficiency from 80% to 90% increases the maximum signal power from ~35kW to ~37.5kW. The impact on the critical pump brightness and minimum required length, core/cladding diameter is also minimal. Finally, varying the pump core absorption (α_{core}), or equivalently the Yb^{3+} concentration, does not change the maximum signal power (see Eq. (12)) and affects only the required core radius (see Eq. (17)) and fiber length (see Eq. (9)).

5. Summary - discussion

In this work, in addition to the commonly used thermal and nonlinear power limiting effects in HPFA power scaling, we have considered the impact of TMI, as well as, further limitations due to bend-induced mechanical reliability and modal deformation.

We have first introduced a simple formula, which provides the MFD shrinkage due to the average heat load in Yb^{3+}-doped fiber amplifiers, and have used it to compare traditional TL power limits to TMI ones. The TMI power limit is shown to be ~35-40% smaller than the TL limit, in very good agreement with experimental results. This demonstrates that TMI occurs before the traditional TL limit is reached and, therefore, dominates power scaling. Using a FIT analysis and considering 1 FIT over 20 years, we have introduced a maximum allowable cladding outer diameter of d_{mech}≈600μm as a new power limiting factor related to the mechanical reliability of bent fibers. This corresponds to a bending diameter of 1m.

Optics EXPRESS

In deriving the TMI threshold we have considered primarily the effects of heat load due to quantum defect. Other parameters, such as gain saturation, higher-order mode excitation at the input and excess signal loss (e.g. due to photodarkening), which are known to affect the TMI threshold have not been taken into account in this study. Any additional factor that reduces the TMI threshold will impact the calculated maximum achievable powers.

We have also introduced the concept of critical pump brightness, which defines the minimum pump brightness needed to reach the maximum achievable signal power. The achievable signal power increases linearly with pump brightness when below the critical value, and remains unchanged above it.

We have used these new findings to investigate the power scaling limits in HPFAs under diode and tandem pumping. In the case of diode pumping, increasing the amplifier gain from 10dB to 20dB increases the maximum signal power from ~27kW to ~38kW. The critical pump brightness in this case increases from 0.18 W/(μm^2 sr) to 0.26 W/(μm^2 sr), and the required core diameter reduces from ~46μm to ~42μm. In the case of tandem pumping, the same amplifier gain variation increases the maximum signal power from ~37kW to ~52kW. The critical pump brightness increases from 0.22 W/(μm^2 sr) to 0.32 W/(μm^2 sr), while the required core diameter reduces from ~62μm to ~55μm. While increasing the amplifier gain results in substantial increase of the maximum achievable signal power, it should be taken into account that high gain amplifiers are more susceptible to back reflections and other external perturbations. As a result, a compromise between highest possible signal power and laser sensitivity to external perturbations should be sought in a robust practical HFFL design.

Although increasing the pump brightness above the critical value does not result in further signal power increase, it reduces considerably the requirements in fiber core/cladding diameters and fiber length leading to more compact and manufacturable HPFLs. Reduced core diameters, e.g. D_{core} < 40-45μm, are more manufacturable with current fiber fabrication techniques and can provide fibers with lower V number and modality. This is beneficial for splicing to SM fibers and for increasing the overall laser efficiency. In addition, as shown in the Fig. 10 inset, reducing the core diameter to D_{core} < 40-45μm results in minimal mode deformation and effective area reduction even with bend diameters in the range of 10-50cm. Reduced cladding diameters, on the other hand, relax the mechanical reliability requirements and allow also for smaller bend diameters (see Fig. 9). This is also known to facilitate bend-induced distributing filtering of HOMs [36], proven to increase the TMI threshold [37] and efficiency of HPFAs with SM output [38].

For an amplifier gain G = 10dB, the maximum achievable signal powers (up to 35kW for DP, and up to 80kW for TP) will require multi-kW pump powers delivered in fibers with maximum cladding diameter of ~600μm and brightness in the range of 0.13-0.26 W/(μm^2 sr) for DP, and 0.14-0.50 W/(μm^2 sr) for TP. Multi-kW pump powers are achieved by combining a number of lower power modules through different incoherent combination techniques [1], such as spatial/polarization geometric combination [39,40], and wavelength beam combination (WBC) [41] or combination of the two [42]. High power pump modules can be potentially further combined by cascaded Nx1 fused tapered fiber bundles [43].

Due to brightness conservation requirements, the pump brightness at the output of an incoherent spatial combiner is always smaller than the brightness of the input pump modules. For DP, current semiconductor diode laser technology can provide geometrically combined multi-element modules with 340W delivered in 105um/0.15NA fibers with brightness of ~0.7 W/(μm^2 sr) [44]. It is questionable though whether spatial incoherent combination of such diode pump modules can provide multi-kW pump power with the required brightness to achieve the predicted maximum signal powers. Alternatively, recent WBC diode technology has demonstrated modules with outputs of 4,680W in 100μm/0.08 NA fiber and record brightness of ~36 W/(μm^2 sr) [41]. This is a promising diode technology for providing the required multi-kW pumps with the brightness to achieve the aforementioned maximum signal powers.

Optics EXPRESS

TP, on the other hand, relies on incoherently combined SM 1018nm fiber lasers to pump a HPFA operating in the 1060nm-1080nm region [2]. It has already been demonstrated that kW-level industrial SM fiber lasers incoherently combined through a cascade of Nx1 fused fiber tapered bundles, can provide 100kW power in 300μm/0.105 NA output fiber with a brightness of ~50 W/(μm^2 sr) [45]. Recently, a 1018nm laser has been demonstrated providing 1,150W output in a 30μm/0.05 NA fiber with brightness of ~207 W/(μm^2 sr) [46]. These results indicate that TP is a mature technology that can provide the required pumping power and brightness to reach the maximum signal powers derived in this work.

Finally, the observed dependencies of minimum core, cladding and fiber length on pump brightness (B_p) (see Fig. 6 and 7) are due to the assumption of constant cladding pump absorption (A_p) and core pump absorption (α_{core}) (or dopant concentration) and a scaling given by Eq. (23). If we assume a different core/cladding scaling, the dopant concentration has to be adjusted appropriately, so that the required A_p and α_{core} are obtained.

Appendix A: Bending-induced mechanical reliability

In all previous power scaling investigations, a fixed core pump absorption (Yb^{3+} concentration) was considered and as a result large core diameters were accompanied by large cladding diameters (>1mm) and long fiber lengths (>>10m) [2–6]. Given that most practical industrial or directed energy HPFL systems should preferably have minimum footprint, the additional constraints of mechanical reliability of bent fibers should be considered. Failure in time (FIT) is calculated by the failure probability, given by [31,32]

$$FIT = \alpha\gamma N_p L \frac{\left(e^n t_s\right)^\beta}{e_p^{n_p} t_p} \tag{21}$$

where

$$\gamma = \left(B_p/E^2\right)/\left(B/E^2\right)^\beta, \qquad e = 0.83 d_{clad}/D_{bend}$$
$$\alpha = m/\left(n_p - 2\right), \qquad \beta = \left(n_p - 2\right)/\left(n - 2\right)$$

with m, N_p, L, E, d_{clad} and D_{bend} being a Weibull distribution constant, failure number per unit amplifier length during proof testing, amplifier length, the fiber elastic modulus, cladding diameter and amplifier bending diameter, respectively. B, n, B_p and n_p, on the other hand, are parameters determined from the crack growth under certain environmental conditions, while e and e_p are applied strain applied and t_s and t_p are times the strain was applied during proof-testing. Typical parameters, used in the calculations, are m = 2.42, N_p = 0.1, L = 10m, n = 20, n_p = 24, e_p = 0.0015, t_p = 1s, t_s = 20years (= 20x31.536x10^{+6}s), and γ = 1000.

Figure 9 shows the calculated failures-in-time (FIT) as a function of fiber bending diameter (D_{bend}), for different cladding diameters. The fiber is assumed to have undergone minimum proof testing and the failure time is 20years [31,32]. Assuming a maximum bending diameter of 1m, the maximum allowable cladding diameter is ~600μm. This limit will be used in the subsequent calculations.

Optics EXPRESS

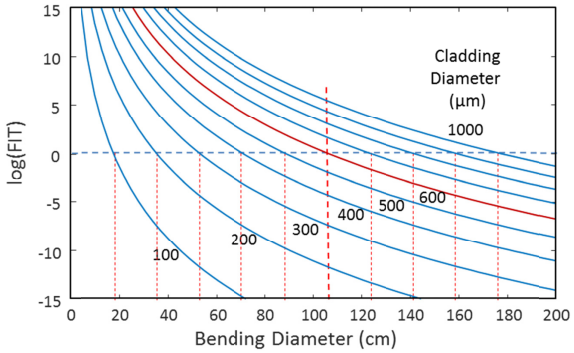

Fig. 9. Failures-in-Time (FIT) versus bending diameter D_{bend-}, for different cladding diameters.

Appendix B: Bend-induced mode field deformation

Bending induced mode field deformation was calculated as a function of the core diameter for different bending diameters. Fiber bending and bend-induced refractive index changes both tend to distort the mode field distributions, and ultimately push the field away from the center of curvature [47].

Figure 10(a) plots the ratio of the fundamental-mode effective area of bent fibers (A_{eff}) over the one of straight fiber (A_{eff}^{∞}) as a function of the core diameter, for different bend diameters. It is shown that increasing the core diameter makes the fiber more susceptible to bending. For a bending diameter of D_{bend}=100cm, a fiber with core diameter D_{core}=50μm suffers an effective area reduction of ~5%, while with D_{core}=100μm suffers a reduction of ~50%. Fig. 10(b) shows representative mode field deformation for core diameter D_{core}=40μm and bending diameter D_{bend}=40cm, 50cm, 70cm and 100cm. They correspond to effective mode area reduction, (defined as $R_{eff}=1-\left(A_{eff}/A_{eff}^{\infty}\right)$, of about 9%, 6%, 3% and 1%, respectively.

Bend-induced modal deformation and effective mode area reduction in multimode fibers is more pronounced for the fundamental mode and has negative impact on the modal competition and overall amplifier efficiency [48]. By setting the effective mode area reduction limit to R_{eff}=10%, from the inset of Fig. 9(a) we conclude that, for a bend diameter D_{bend}=100cm, the maximum tolerable core diameter is ~55μm. If we consider smaller core diameters in the range of 25μm-45μm, on the other hand, the allowable bending diameter reduces to D_{bend}=10cm-50cm. This potentially results in more compact designs with smaller footprint.

Optics EXPRESS

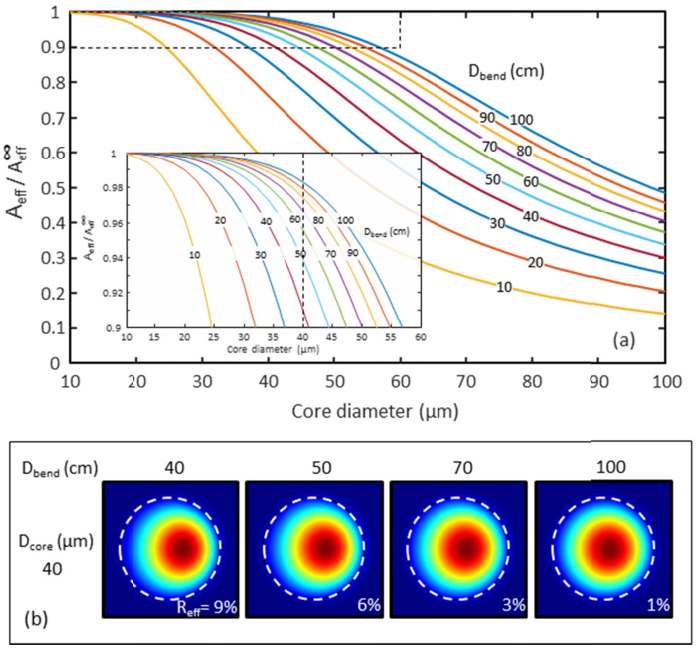

Fig. 10. (a) Mode field deformation for core diameter D_{core} = 40μm and bending diameter D_{bend} = 40cm, 50cm, 70cm and 100cm; (b) Mode effective area ratio versus core diameter for different bending diameters (V = 6). The inset zooms into the top-left highlighted area.

Appendix C: Nonlinear and other power limit formulae [J. W. Dawson, Opt. Express 16(17), 13240–13266 (2008)]

C.1. Pump power limit

$$P_{out}^{pump} = \eta_{laser} B_p \left(\pi r_{clad}^2\right)\left(\pi NA^2\right) = \eta_{laser} B_p \pi^2 NA^2 r_0^2 \frac{\alpha_{core}}{A_p} L, \tag{22}$$

where $A_p = \alpha_{clad} L$ (in dB) is the small-signal total pump absorption and $\alpha_{clad} = \alpha_{core}\left(r_0/r_{clad}\right)^2$ small-signal cladding pump absorption coefficient (in dB/m) and α_{core} the small-signal pump core absorption coefficient (in dB/m). r_0 and r_{clad} are the core and cladding radii. η_{laser} is the pump-to-signal conversion efficiency. L is the fiber length.

For given α_{core}, α_{clad} (in dB/m) and L, the required cladding diameter d_{clad} is given by:

$$d_{clad} = d_0 \sqrt{\alpha_{core}/\alpha_{clad}} = d_0 \sqrt{\alpha_{core} L / A_p} \tag{23}$$

where $d_{\text{clad}} = 2r_{\text{clad}}$ and $d_0 = 2r_0$.

C.2. TMI Power limit [M. N. Zervas, Proc. SPIE 10083, 100830M (2017)]

$$P_{out}^{TMI} = \frac{\kappa U_\varepsilon^2 \left(U_\varepsilon^2 - U_s^2\right)}{4\pi n_{eff} \alpha_s' \left(dn/dT\right)} \left(\frac{\lambda_0}{d_0}\right)^2 \tag{24}$$

where $\alpha_s' = \alpha_s + 0.5 q_D g_s$ is a heat generation coefficient. α_s includes the signal background loss and other contributions, such as phorodarkening, while $q_D g_s$ describes the heat generation coefficient due to quantum defect ($q_D = \lambda_s/\lambda_p - 1$) and gain saturation ($g_s$). κ is the silica

Optics EXPRESS

thermal conductivity and dn/dT the thermo-optic coefficient. $d_0 = 2r_0$ is the core diameter. n_{eff} is the fundamental mode effective index and $U_s(U_\varepsilon)$ is the normalized transverse wavenumber for the fundamental (higher-order) fiber mode, approximated by $U_{s(\varepsilon)}(V) = U_{s(\varepsilon)}(\infty)\exp(-1/V)$, where the asymptotic values for LP_{01} and LP_{11} mores are $U_s(\infty) = 2.405$ and $U_\varepsilon(\infty) = 3.832$, respectively, and V is the core V-number [49].

C.3. Thermal lens power limit

$$P_{out}^{TL} = \frac{2\pi\kappa}{\left[\eta_{heat}/(\eta_{laser}L)\right](dn/dT)}\left(\frac{\lambda_0}{d_0}\right)^2 \tag{25}$$

where η_{heat} is the fraction of power turned into heat inside the core, due to the quantum defect and other contributions (such as background signal loss and photodarkening).

C.4. Stimulated Raman scattering (SRS) power limit

$$P_{out}^{SRS} \approx \frac{16A_{eff}G}{g_R L_{eff}} = \frac{16\pi r_0^2\Gamma^2\ln(G)}{g_R L}, \tag{26}$$

where $A_{eff} = \Gamma^2\pi r_0^2 = \pi r_{MF}^2$, $L_{eff} = \frac{1}{g_s}\left(e^{g_s L} - 1\right)$, $g_s = \ln(G)/L$ and G is the amplifier single-pass saturated average gain. $r_{MF} = r_0\Gamma$ is the mode field radius.

C.5. Optical damage power limit

$$P_{out}^{damage} = I_{damage}\Gamma^2\pi r_0^2 \tag{27}$$

where I_{damage} is the damage intensity.

C.6. Thermal rapture power limit

$$P_{out}^{rupture} = \frac{\eta_{laser}}{\eta_{heat}}\frac{4\pi R_m}{1 - \frac{r_0^2}{2r_{clad}^2}}L \tag{28}$$

where R_{m} is the rupture modulus of silica glass and r_{clad} is the cladding diameter.

C.7. Core melting power limit

$$P_{out}^{melting} = \frac{\eta_{laser}}{\eta_{heat}}\frac{4\pi\kappa(T_m - T_c)}{1 + \frac{2\kappa}{r_{clad}h} + 2\ln\left(\frac{r_{clad}}{r_0}\right)}L \tag{29}$$

where T_{m} is the melt temperature of fused silica, T_{c} is the coolant temperature and h is the convective coefficient.

Typical parameter values are given in Table 1.

Optics EXPRESS

Table 1: List of parameters, symbols used in the text and values used in the calculations

Parameter	Symbol	Value	Units
Rupture modulus (SiO_2)	R_m	2460	W/m
Optical Damage Intensity	I_{damage}	30	$W/\mu m^2$
Thermal Conductivity (SiO_2)	κ	1.38	W/(m-K)
Convective film cooling coefficient	h	10,000	$W/(m^2-K)$
Laser Coolant Temperature	T_c	300	K
Melt Temperature (SiO_2)	T_m	1983	K
Thermo-optic Coefficient	dn/dT	$1.18x10^{-5}$	1/K
Peak Raman gain coefficient	g_R	$1x10^{-13}$	m/W
Small-Signal Pump Absorption	A_p	20	dB
Fiber normalised frequency	V	3	
Amplifier Gain	G	10-100	
MFD/Core Radius Ratio	Γ	0.8	
Peak Pump Core Absorption (Diode Pumping)	α_{core}	250	dB/m
(Tandem Pumping)		100	
Yb^{3+} Concentration (Diode Pumping)	N_0	$2.65x10^{+25}$	m^{-3}
(Tandem Pumping)		$4.6x10^{+26}$	
Heat Conversion Coefficient (Diode Pumping)	η_{heat}	0.10	
(Tandem Pumping)		0.06	

Appendix D: Heat-induced fundamental mode MFD shrinkage in optical fibers

As already mentioned, in previous studies [3], the TL power limit (see Eq. (6)) corresponds to ~20-30% MFD reduction of a Gaussian beam propagating in free space. We can now use the simplified analysis and results of Sections 2.1 and 2.2 to derive the corresponding MFD reduction in optical fibers at the TL power limit.

From Eqs.. (3), (4) and (6), setting $P_s = P_{out}^{TL}$, the peak of the thermally-induced quasi-parabolic RI profile in the "hot" fiber is given by:

$$\Delta n_{th}^{TL} = \frac{1}{2}\left(\frac{\lambda_0}{d_0}\right)^2 \tag{30}$$

From Eq. (5), the corresponding "hot" fiber normalized MFD is approximated by:

$$\frac{\omega_{th}^{TL}}{d_0} \simeq \sqrt{\frac{2}{V_{th}^{TL}}} \tag{31}$$

where $V_{th}^{TL} = V\sqrt{1+\Delta n_{th}^{TL}/\Delta n}$. From the "cold" fiber V-number definition, on the other hand, we obtain $\Delta n = \left(V^2/2n_2\pi^2\right)\left(\lambda_0/d_0\right)^2$, which for typical V = 3-4 is approximated by

Optics EXPRESS

$\Delta n \simeq (1/2)(\lambda_0/d_0)^2 = \Delta n_{th}^{TL}$ and results in $V_{th}^{TL} \simeq V\sqrt{2}$. For V = 3-4, on the other hand, Eq. (1) results in $(\omega_0/d_0) \simeq 1$ for the "cold" fiber normalized MFD.

Under these approximations, the "hot"-to-"cold" fiber fundamental mode MFD ratio is given by:

$$\frac{\omega_{th}^{TL}}{\omega_0} \simeq \sqrt{\frac{\sqrt{2}}{V}} \tag{32}$$

which for V = 3-4 results in $\omega_{th}^{TL}/\omega_0 \simeq 0.7-0.8$. It is shown that at the TL power limit, given by Eq. (6), the optical fiber fundamental mode MFD shrinkage is similar to the one considered in Gaussian mode free-space propagation [3].

Funding

EPSRC (EP/P027644/1; EP/N00762X/1); Royal Academy of Engineering (Research Chairs and Senior Research Fellowships Scheme).

Acknowledgements

Special thanks go to Dr. Natasha Vukovic for the bending-induced mode field deformation calculations, and Dr. C. A. Codemard for useful discussions. The data can be found in https://doi.org/10.5258/SOTON/D0923.

References

1. M. N. Zervas and C. A. Codemard, "High Power Fiber Lasers: A Review," IEEE J. Sel. Top. Quantum Electron. **20**(5), 0904123 (2014).
2. M. O'Connor and B. Shiner, "High power fiber lasers for industry and defense," in *High-Power Laser Handbook*, H. Injeyan, G.D. Goodno (Eds), (McGraw Hill, 2011), Ch. 18.
3. J. W. Dawson, M. J. Messerly, R. J. Beach, M. Y. Shverdin, E. A. Stappaerts, A. K. Sridharan, P. H. Pax, J. E. Heebner, C. W. Siders, and C. P. J. Barty, "Analysis of the scalability of diffraction-limited fiber lasers and amplifiers to high average power," Opt. Express **16**(17), 13240–13266 (2008).
4. J. W. Dawson, M. J. Messerly, J. E. Heebner, P. H. Pax, A. K. Sridharan, A. L. Bullington, R. J. Beach, C. W. Siders, C. P. J. Barty, and M. Dubinskii, "Power scaling analysis of fiber lasers and amplifiers based on nonsilica materials," Proc. SPIE **7686**, 768611 (2010).
5. J. Zhu, P. Zhou, Y. Ma, X. Xu, and Z. Liu, "Power scaling analysis of tandem-pumped Yb-doped fiber lasers and amplifiers," Opt. Express **19**(19), 18645–18654 (2011).
6. W.-W. Ke, X.-J. Wang, X.-F. Bao, and X.-J. Shu, "Thermally induced mode distortion and its limit to power scaling of fiber lasers," Opt. Express **21**(12), 14272–14281 (2013).
7. T. Eidam, C. Wirth, C. Jauregui, F. Stutzki, F. Jansen, H.-J. Otto, O. Schmidt, T. Schreiber, J. Limpert, and A. Tünnermann, "Experimental observations of the threshold-like onset of mode instabilities in high power fiber amplifiers," Opt. Express **19**(14), 13218–13224 (2011).
8. H.-J. Otto, C. Jauregui, J. Limpert, and A. Tünnermann, "Average power limit of Ytterbium-doped fiber-laser systems with nearly diffraction-limited beam quality," Proc. SPIE **9728**, 97280E (2016).
9. M. N. Zervas, "Power scalability in high power fiber amplifiers," in *Conference on Lasers and Electro-Optics Europe & European Quantum Electronics Conference (CLEO/Europe-EQEC)* (IEEE, 2017) paper CJ-6.1.
10. M. N. Zervas, "Power scaling limits in high power fiber amplifiers due to transverse mode instability, thermal lensing, and fiber mechanical reliability," Proc. SPIE **10512**, 10501205 (2018).
11. C. Jauregui, H.-J. Otto, S. Breitkopf, J. Limpert, and A. Tünnermann, "Optimizing high-power Yb-doped fiber amplifier systems in the presence of transverse mode instabilities," Opt. Express **24**(8), 7879–7892 (2016).
12. F. Stutzki, F. Jansen, A. Liem, C. Jauregui, J. Limpert, and A. Tünnermann, "26 mJ, 130 W Q-switched fiber-laser system with near-diffraction-limited beam quality," Opt. Lett. **37**(6), 1073–1075 (2012).
13. A. Steinkopff, C. Jauregui, F. Stutzki, J. Nold, C. Hupel, N. Haarlammert, J. Bierlich, A. Tünnermann, and J. Limpert, "Transverse single-mode operation in a passive large pitch fiber with more than 200 µm mode-field diameter," Opt. Lett. **44**(3), 650–653 (2019).
14. F. Jansen, F. Stutzki, H.-J. Otto, T. Eidam, A. Liem, C. Jauregui, J. Limpert, and A. Tünnermann, "Thermally induced waveguide changes in active fibers," Opt. Express **20**(4), 3997–4008 (2012).
15. M. N. Zervas, "TMI threshold in high power fiber amplifiers," in *OSA Advanced Photonics Congress* (Optical Society for America, 2016), paper SoW2H.2.
16. M. N. Zervas, "Transverse mode instability analysis in fiber amplifiers," Proc. SPIE **10083**, 100830M (2017).

Optics EXPRESS

17. M. N. Zervas, "Transverse-modal-instability gain in high power fiber amplifiers: effect of the perturbation relative phase," APL Photonics **4**(2), 022802 (2019).
18. Y. Jeong, J. Sahu, D. Payne, and J. Nilsson, "Ytterbium-doped large-core fiber laser with 1.36 kW continuous-wave output power," Opt. Express **12**(25), 6088–6092 (2004).
19. J. D. Minelly, R. I. Laming, J. E. Townsend, W. L. Barnes, E. R. Taylor, K. P. Jedrzejewski, and D. N. Payne, "High gain fibre power amplifier tandem-pumped by a 3 W multistripe diode," in *Conference on Optical Fiber Communication* (Optical Society of America, 1992), pp. 32–33.
20. C. A. Codemard, J. K. Sahu, and J. Nilsson, "Tandem cladding-pumping for control of excess gain in ytterbium-doped fiber amplifiers," IEEE J. Quantum Electron. **46**(12), 1860–1869 (2010).
21. D. Marcuse, "Loss analysis of single-mode fiber splices," Bell Syst. Tech. J. **56**(5), 703–718 (1977).
22. K. R. Hansen, T. T. Alkeskjold, J. Broeng, and J. Lægsgaard, "Theoretical analysis of mode instability in high-power fiber amplifiers," Opt. Express **21**(2), 1944–1971 (2013).
23. D. C. Brown and H. J. Hoffman, "Thermal, Stress, and Thermo-Optic Effects in High Average Power Double-Clad Silica Fiber Lasers," IEEE J. Quantum Electron. **37**(2), 207–217 (2001).
24. F. Stutzki, F. Jansen, H.-J. Otto, C. Jauregui, J. Limpert, and A. Tünnermann, "Designing advanced very-large mode-area fibers for power scaling of fiber-laser systems," Optica **1**(4), 233–242 (2014).
25. F. Stutzki, F. Jansen, A. Liem, C. Jauregui, J. Limpert, and A. Tünnermann, "26 mJ, 130 W Q-switched fiber-laser system with near-diffraction-limited beam quality," Opt. Lett. **37**(6), 1073–1075 (2012).
26. O. Antipov, M. Kuznetsov, D. Alekseev, and V. Tyrtyshnyy, "Influence of a backward reflection on low-threshold mode instability in Yb3+-doped few-mode fiber amplifiers," Opt. Express **24**(13), 14871–14879 (2016).
27. Z. Li, Z. Huang, X. Xiang, X. Liang, H. Lin, S. Xu, Z. Yang, J. Wang, and F. Jing, "Experimental demonstration of transverse mode instability enhancement by a counter-pumped scheme in a 2 kW all-fiberized laser," Photon. Res. **5**(2), 77–81 (2017).
28. M. Laurila, M. M. Jørgensen, K. R. Hansen, T. T. Alkeskjold, J. Broeng, and J. Lægsgaard, "Distributed mode filtering rod fiber amplifier delivering 292W with improved mode stability," Opt. Express **20**(5), 5742–5753 (2012).
29. M. M. Johansen, K. R. Hansen, M. Laurila, T. T. Alkeskjold, and J. Lægsgaard, "Estimating modal instability threshold for photonic crystal rod fiber amplifiers," Opt. Express **21**(13), 15409–15417 (2013).
30. M. Walorny, J. Abramczyk, N. Jacobson, and K. Tankala, "Mechanical reliability of double clad fibers in typical fiber laser deployment conditions," Proc. SPIE **9728**, 97283A (2016).
31. Y. Mitsunaga, Y. Katsuyama, H. Kobayashi, and Y. Ishida, "Failure prediction for long length optical fiber based on proof testing," J. Appl. Phys. **53**(7), 4847–4853 (1982).
32. M. Yamada, K. Tsujikawa, L. Ma, K. Ichii, S. Matsuo, N. Hanzawa, and H. Ono, "Optical fiber amplifier employing a bundle of reduced cladding erbium-doped fibers," IEEE Photonics Technol. Lett. **24**(21), 1910–1913 (2012).
33. F. Beier, C. Hupel, S. Kuhn, S. Hein, J. Nold, F. Proske, B. Sattler, A. Liem, C. Jauregui, J. Limpert, N. Haarlammert, T. Schreiber, R. Eberhardt, and A. Tünnermann, "Single mode 4.3 kW output power from a diode-pumped Yb-doped fiber amplifier," Opt. Express **25**(13), 14892–14899 (2017).
34. T. Yao, J. Ji, and J. Nilsson, "Ultra-low quantum defect heating in Ytterbium-doped aluminosilicate fibers," J. Lightwave Technol. **32**(3), 429–434 (2014).
35. H.-J. Otto, N. Modsching, C. Jauregui, J. Limpert, and A. Tünnermann, "Impact of photodarkening on the mode instability threshold," Opt. Express **23**(12), 15265–15277 (2015).
36. J. P. Koplow, D. A. V. Kliner, and L. Goldberg, "Single-mode operation of a coiled multimode fiber amplifier," Opt. Lett. **25**(7), 442–444 (2000).
37. A. V. Smith and J. J. Smith, "Mode instability thresholds of fiber amplifiers," Proc. SPIE **8601**, 860108 (2013).
38. L. Huang, L. Kong, J. Leng, P. Zhou, S. Guo, and X. Cheng, "Impact of high-order-mode loss on high-power fiber amplifiers," J. Opt. Soc. Am. B **33**(6), 1030–1037 (2016).
39. T. Y. Fan, "Efficient coupling of multiple diode laser arrays to an optical fiber by geometric multiplexing," Appl. Opt. **30**(6), 630–632 (1991).
40. K. Price, S. Karlsen, P. Leisher, and R. Martinsen, "High-brightness fiber-coupled pump laser development," Proc. SPIE **7583**, 758308 (2010).
41. R. K. Huang, B. Chann, J. Burgess, B. Lochman, W. Zhou, M. Cruz, R. Cook, D. Dugmore, J. Shattuck, and P. Tayebati, "TeraDiode's high brightness semiconductor lasers," Proc. SPIE **9730**, 97300C (2016).
42. M. Hemenway, Z. Chen, M. Kanskar, W. Urbanek, D. Dawson, L. Bao, M. DeFranza, M. DeVito, K. Fortier, R. Martinsen, and K. Welch, "976nm high brightness fiber-coupled laser modules for ytterbium fiber laser pumping," Proc. SPIE **10900**, 109000D (2019).
43. C. Headley III, M. Fishteyn, A. D. Yablon, M. J. Andrejco, K. Brar, J. Mann, M. D. Mermelstein, and D. J. DiGiovanni, "Tapered fiber bundles for combining laser pumps," Proc. SPIE **5709**, 263–272 (2005).
44. M. Kanskar, C. Bai, L. Bao, N. Biekert, Z. Chen, M. DeFranza, M. DeVito, K. Fortier, M. Grimshaw, X. Guan, M. Hemenway, S. Li, E. Martin, R. Martinsen, T. Prunty, W. Urbanek, B. Wilkins, J. Zhang, and S. Zhang, "High Brightness Diodes and 600 W & 60% Efficient Low SWaP Fiber-coupled Package Enabled by Reduced-mode (REM) Diodes," Proc. SPIE **10900**, 109000H (2019).

Optics EXPRESS

45. E.A. Shcherbakov, V.V. Fomin, A.A. Abramov, A.A. Ferin, D.V. Mochalov, and V. P. Gapontsev, "Industrial grade 100 kW power CW fiber laser," in *Advanced Solid-State Lasers Congress* (Optical Society of America, 2013), paper ATh4A.2.
46. P. Yan, X. Wang, Z. Wang, Y. Huang, D. Li, Q. Xiao, and M. Gong, "A 1150-W 1018-nm fiber laser bidirectional pumped by wavelength-stabilized laser diodes," IEEE J. Sel. Top. Quantum Electron. **24**(3), 0902506 (2018).
47. D. Marcuse, "Field deformation and loss caused by curvature of optical fibers," J. Opt. Soc. Am. **66**(4), 311–320 (1976).
48. J. M. Fini, "Design of large-mode-area amplifier fibers resistant to bend-induced distortion," J. Opt. Soc. Am. B **24**(8), 1669–1676 (2007).
49. A. W. Snyder, "Asymptotic expressions for eigenfunctions and eigenvalues of a dielectric or optical waveguide," IEEE Trans. Microw. Theory Tech. **17**(12), 1130–1138 (1969).